Inorg. Chem. **2005**, *44*, 2391–2399

Magneto–Structural Correlations: Synthesis of a Family of End-On Azido-Bridged Manganese(II) Dinuclear Compounds with $S = 5$ Spin Ground State

Tapan K. Karmakar,[†] Barindra K. Ghosh,[†] A. Usman,[‡] Hoong-Kun Fun,[‡] Eric Rivière,[§] Talal Mallah,[§] Guillem Aromí,*[,||] and Swapan K. Chandra*[,†,⊥]

Department of Chemistry, The University of Burdwan, Burdwan-713104, India, X-ray Crystallography Unit, School of Physics, Universiti Sains Malaysia, 11800 USM, Penang, Malaysia, Laboratoire de Chimie Inorganique, Universite Paris-Sud, Bat. 420, UMR CNRS 8613, 91405 Orsay, France, and Departament de Química Inorgànica, Facultat de Química, Universitat de Barcelona, Diagonal 647, 08028 Barcelona, Spain

Received October 18, 2004

The preparation of a series of multidentate pyridyl–imine ligands, L1–L3, and their reactivity with the Mn^{II}/N_3^- system is described (L1 = [*N*,*N*-bis(pyridine-2-yl)benzylidene]ethane-1,2-diamine; L2 = [*N*,*N*-bis(pyridine-2-yl)-benzylidene]propane-1,3-diamine, and L3 = [*N*,*N*-bis(pyridine-2-yl)benzylidene]butane-1,4-diamine). Complexes comprising dinuclear end-on bis(μ-azido)-bridged manganese(II) units of formulas $[Mn_2(L1)_2(N_3)_4][Mn_2(L1)_2(N_3)_2(CH_3OH)_2](ClO_4)_2$ (two cocrystallized dinuclear units, **1·2**), $[Mn_2(L2)_2(N_3)_2](ClO_4)_2$ (**3**), and $[Mn_2(L3)_2(N_3)_2](ClO_4)_2$ (**4**) have been synthesized. The crystal structures of complexes **1**–**4** as well as their magnetic properties are presented. Each manganese atom of cocrystallized complexes in compound **1·2** is heptacoordinated, displaying Mn–N–Mn angles, θ, of 102.53(12) and 101.70(12)° and Mn···Mn distances of 3.5091(7) and 3.4680(7) Å. On the other hand, each manganese center in compounds **3** and **4** is located within an octahedral coordination environment, the complexes displaying θ angles of 104.29(11) and 103.60(18)°, respectively, and Mn···Mn vectors of 3.5371(7) and 3.5338(10) Å, respectively. Magnetic susceptibility studies revealed the presence of intramolecular ferromagnetic superexchange, yielding an $S = 5$ spin ground state in all complexes. Fitting of the experimental data led to coupling constants, intermolecular exchange values, and *g* factors (in the *J*/*zJ*′/*g* format) of 0.77 cm^{-1}/0.01 cm^{-1}/2.20 (**1·2**), 2.04 cm^{-1}/0.01 cm^{-1}/1.99 (**3**), and 1.75 cm^{-1}/–0.05 cm^{-1}/2.04 (**4**), respectively (using $H = -2JS_1S_2$ as the convention for the Heisenberg spin-Hamiltonian). These results are consistent with predictions from recent DFT calculations performed on end-on bis(μ-N_3^-)-bridged Mn^{II} dinuclear complexes. A plot of experimental *J* vs θ, including data from the only preexisting compound of this kind, reveals a linear relationship, which could be the first evidence of a possible magneto–structural correlation between these two parameters.

Introduction

The area of molecular magnetism has stimulated for many years great efforts from the synthetic arena of coordination chemistry with the goal of preparing materials with the desired magnetic properties. In this respect, the judicious choice of ligands intended to propagate specific magnetic interactions has been a successful approach.[1,2] Another resource often incorporated into synthetic strategies has been the preparation and use of polynucleating ligands aimed at the formation of metal cages with specific topologies,[3−5] sometimes in combination with the above methodology.[6] This activity has experienced added impetus since the advent of

* Authors to whom correspondence should be addressed. E-mail: dr_swapan@sify.com (S.K.C.); guillem.aromi@qi.ub.es (G.A.).
[†] The University of Burdwan.
[‡] Universiti Sains Malaysia.
[§] Universite Paris-Sud.
[||] Universitat de Barcelona.
[⊥] Present address: Department of Chemistry, Visva Bharati Santiniketan, 731 235 India.

(1) Ferlay, S.; Mallah, T.; Ouahes, R.; Veillet, P.; Verdaguer, M. *Nature* **1995**, *378*, 701.
(2) Papaefstathiou, G. S.; Perlepes, S. P.; Escuer, A.; Vicente, R.; Font-Bardia, M.; Solans, X. *Angew. Chem., Int. Ed.* **2001**, *40*, 884.
(3) Dapporto, P.; Formica, M.; Fusi, V.; Micheloni, M.; Paoli, P.; Pontellini, R.; Rossi, P. *Inorg. Chem.* **2000**, *39*, 4663.
(4) Aromí, G.; Ribas, J.; Gamez, P.; Roubeau, O.; Kooijman, H.; Spek, A. L.; Teat, S.; MacLean, E.; Stoeckli-Evans, H.; Reedijk, J. *Chem.—Eur. J.* **2004**, *10*, 6476.

10.1021/ic048542v CCC: $30.25
Published on Web 02/25/2005

single molecule magnets (SMMs).[7,8] These are molecules that can be magnetized individually below a blocking temperature and, therefore, offer the potential of being used as molecular devices for the storage of magnetic information. To show these properties such species must possess a relatively large spin ground state, S_T, and significant easy-axis magnetic anisotropy reflected in a large zero field splitting (ZFS) parameter D.[9,10] Since this discovery, a few compounds of this type have been prepared, all involving open-shell transition metals. Thus, SMMs of Mn (the vast majority),[11,12] Fe,[13] Co,[14] and Ni[15] are known today, as well as two examples of 3d−4f heterometallic compounds.[16,17a,17b] Increasing the size of this family remains important, since it is essential for gaining deeper insight into the phenomenon.

The goal of achieving high S_T values must be fulfilled through magnetic superexchange between spin carriers within molecules. This can take place as a result of antiferromagnetic coupling between individual spin moments without total cancellation, leading to a nonzero net magnetic moment of the molecule, or from alignment of the spins contained in the cluster through ferromagnetic coupling. Ferromagnetic interactions are much more rare than antiferromagnetic and remain a pathway into SMMs that has been insufficiently exploited. In particular, generation of systems involving such exchange between high-spin Mn^{II} centers is particularly desirable since this ion contains the highest possible number of unpaired electrons for a 3d metal, five, with an individual spin of $S = 5/2$. In this context, the exploration of the bridging potential of the azido ligand seems very appropriate; it shows a large variety of bridging modes and has been know for a long time to efficiently mediate magnetic coupling between paramagnetic centers. The most commonly observed ways of bridging are (see Chart 1) as μ-η^1-N_3^- (end-on)[18−21] and μ-$\eta^{1,3}$-N_3^- (end-to-end),[22−24] usually facilitating ferro- and antiferromagnetic exchange, respectively, although examples of ferromagnetic coupling via end-to-end bridges have also been reported.[25,26] Prediction of the bridging mode that will be adopted is very difficult, although in some cases the use of appropriate coligands can help to influence the form that will be observed. The ferromagnetic nature of the exchange within end-on azido-bridged Cu^{II} and Ni^{II} dinuclear complexes is well documented and has been illustrated with numerous examples. It is surprising, however, to observe the paucity with which analogous systems comprising Mn^{II} have been appearing in the literature, with only one such example reported hitherto.[27]

Chart 1

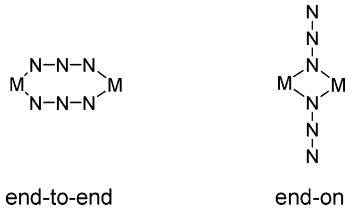

In this paper we describe the preparation of a series of flexible multidentate ligands, L1−L3 (Chart 2), based on imine and pyridine functionalities, which have shown the ability of stabilizing pairs of Mn^{II} ions in the presence of azido ions. Thus, a family of bis(μ-η^1-N_3^-)-bridged dinuclear complexes has been prepared, with formulas $[Mn_2(L1)_2(N_3)_4]$-$[Mn_2(L1)_2(N_3)_2(CH_3OH)_2](ClO_4)_2$ (**1·2**), $[Mn_2(L2)_2(N_3)_2]$-$(ClO_4)_2$ (**3**), and $[Mn_2(L3)_2(N_3)_2](ClO_4)_2$ (**4**). The structures of complexes **1**−**4** are described herein, along with their bulk magnetic properties. The data arising from this work have allowed, in combination with the only previously reported case, us to investigate the possible relationship between the magnetic behavior and structural parameters. This has revealed a linear dependence of the coupling constant J with

Chart 2

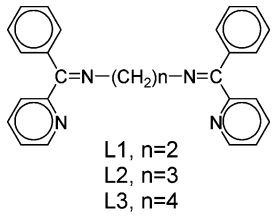

(5) Zhao, L.; Xu, Z. Q.; Grove, H.; Milway, V. A.; Dawe, L. N.; Abedin, T. S. M.; Thompson, L. K.; Kelly, T. L.; Harvey, R. G.; Miller, D. O.; Weeks, L.; Shapter, J. G.; Pope, K. J. *Inorg. Chem.* **2004**, *43*, 3812.
(6) Abbati, G. L.; Cornia, A.; Caneschi, A.; Fabretti, A. C.; Mortalo, C. *Inorg. Chem.* **2004**, *43*, 4540.
(7) Sessoli, R.; Tsai, H. L.; Schake, A. R.; Wang, S. Y.; Vincent, J. B.; Folting, K.; Gatteschi, D.; Christou, G.; Hendrickson, D. N. *J. Am. Chem. Soc.* **1993**, *115*, 1804.
(8) Sessoli, R.; Gatteschi, D.; Caneschi, A.; Novak, M. A. *Nature* **1993**, *365*, 141.
(9) Christou, G.; Gatteschi, D.; Hendrickson, D. N.; Sessoli, R. *MRS Bull.* **2000**, *25*, 66.
(10) Gatteschi, D.; Sessoli, R. *Angew. Chem., Int. Ed.* **2003**, *42*, 268.
(11) Brechin, E. K.; Boskovic, C.; Wernsdorfer, W.; Yoo, J.; Yamaguchi, A.; Sañudo, E. C.; Concolino, T. R.; Rheingold, A. L.; Ishimoto, H.; Hendrickson, D. N.; Christou, G. *J. Am. Chem. Soc.* **2002**, *124*, 9710.
(12) Tasiopoulos, A. T.; Vinslava, A.; Wernsdorfer, W.; Abboud, K. A.; Christou, G. *Angew. Chem., Int. Ed.* **2004**, *43*, 2117.
(13) Gatteschi, D.; Sessoli, R.; Cornia, A. *Chem. Commun.* **2000**, 725.
(14) Murrie, M.; Teat, S. J.; Stoeckli-Evans, H.; Gudel, H. U. *Angew. Chem., Int. Ed.* **2003**, *42*, 4653.
(15) Andres, H.; Basler, R.; Blake, A. J.; Cadiou, C.; Chaboussant, G.; Grant, C. M.; Güdel, H. U.; Murrie, M.; Parsons, S.; Paulsen, C.; Semadini, F.; Villar, V.; Wernsdorfer, W.; Winpenny, R. E. P. *Chem.—Eur. J.* **2002**, *8*, 4867.
(16) Osa, S.; Kido, T.; Matsumoto, N.; Re, N.; Pochaba, A.; Mrozinski, J. *J. Am. Chem. Soc.* **2004**, *126*, 420.
(17) (a) Zaleski, C. M.; Depperman, E. C.; Kampf, J. W.; Kirk, M. L.; Pecoraro, V. L. *Angew. Chem., Int. Ed.* **2004**, *43*, 3912. (b) For a recent third example of mixed 3d−4f single-molecule magnet see: Mishra, A.; Wernsdorfer, W.; Abboud, K. A.; Christou, G. *J. Am. Chem. Soc.* **2004**, *126*, 15648.
(18) Cortes, R.; Delarramendi, J. I. R.; Lezama, L.; Rojo, T.; Urtiaga, K.; Arriortua, M. I. *J. Chem. Soc., Dalton Trans.* **1992**, 2723.
(19) Escuer, A.; Vicente, R.; Ribas, J.; Solans, X. *Inorg. Chem.* **1995**, *34*, 1793.
(20) Barandika, M. G.; Cortes, R.; Lezama, L.; Urtiaga, M. K.; Arriortua, M. I.; Rojo, T. *J. Chem. Soc., Dalton Trans.* **1999**, 2971.
(21) Cano, J.; De Munno, G.; Lloret, F.; Julve, M. *Inorg. Chem.* **2000**, *39*, 1611.
(22) Escuer, A.; Castro, I.; Mautner, F.; ElFallah, M. S.; Vicente, R. *Inorg. Chem.* **1997**, *36*, 4633.
(23) Escuer, A.; Vicente, R.; El Fallah, M. S.; Solans, X.; Font-Bardia, M. *Inorg. Chim. Acta* **1998**, *278*, 43.
(24) Maji, T. K.; Mukherjee, P. S.; Koner, S.; Mostafa, G.; Tuchagues, J. P.; Chaudhuri, N. R. *Inorg. Chim. Acta* **2001**, *314*, 111.
(25) Maji, T. K.; Mukherjee, P. S.; Mostafa, G.; Mallah, T.; Cano-Boquera, J.; Chaudhuri, N. R. *Chem. Commun.* **2001**, 1012.
(26) Hong, C. S.; Koo, J. E.; Son, S. K.; Lee, Y. S.; Kim, Y. S.; Do, Y. *Chem.—Eur. J.* **2001**, *7*, 4243.
(27) Cortes, R.; Pizarro, J. L.; Lezama, L.; Arriortua, M. I.; Rojo, T. *Inorg. Chem.* **1994**, *33*, 2697.

respect to the Mn−N−Mn bridging angle, θ, in what could be the first manifestation of a magneto−structural correlation for this type of system.

Experimental Section

Syntheses. All manipulations were performed under aerobic conditions using reagents and solvents as received.

Ligands. [*N*,*N*-Bis(pyridine-2-yl)benzylidene]ethane-1,2-diamine (L1), [*N*,*N*-bis(pyridine-2-yl)benzylidene]propane-1,3-diamine (L2), and [*N*,*N*-bis(pyridine-2-yl)benzylidene]butane-1,4-diamine (L3) were prepared via condensation reactions similar to previously reported for a similar ligand.[28] Ethylenediamine (0.60 g, 10 mmol, L1), 1,3-diaminopropane (0.74 g, 10 mmol, L2), or 1,4-diaminobutane (0.88 g, 10 mmol, L3) and 2-benzoylpyridine (3.66 g, 20 mmol) were refluxed in 15 mL of dehydrated alcohol for 6 h and cooled to room temperature. In each case the resulting brown solution was filtered, and the solvent from the filtrate was removed by rotary evaporation. The brown semisolid mass was then redissolved in hot ethanol (∼20 mL), and hot water (about 5−8 mL) was added dropwise until precipitation occurred. This mixture was heated to get a clear solution and cooled in an ice bath. The products were isolated as a brown waxy materials after drying in a vacuum over P_4O_{10}. The yields were 3.50 g (∼90%), 3.60 g (∼89%), and 4.00 g (∼96%) for L1−L3, respectively. Anal. Calcd for $C_{26}H_{22}N_4$ (L1): C, 79.97; H, 5.68; N, 14.35. Found: C, 79.92; H, 5.51; N, 14.19. Calcd for $C_{27}H_{24}N_4$ (L2): C, 80.17; H, 5.98; N, 13.85. Found: C, 79.97; H, 5.81; N, 13.69. Calcd for $C_{28}H_{26}N_4$ (L3): C, 80.35; H, 6.26; N, 13.38. Found: C, 80.17; H, 6.31; N, 13.25.

Complexes. (i) $[Mn_2(L1)_2(N_3)_4][Mn_2(L1)_2(N_3)_2(CH_3OH)_2](ClO_4)_2$ (1·2). To a methanolic solution (15 mL) of $Mn(ClO_4)_2\cdot 6H_2O$ (0.36 g, 1.0 mmol) was added L1 (0.390 g, 1.0 mmol) in acetonitrile (5 mL) over a period of 15 min. To the resulting yellow-orange solution was added slowly an aqueous methanolic solution (3 mL of H_2O and 7 mL of MeOH) of sodium azide (0.098 g, 1.5 mmol). The solution was then filtered, an insoluble precipitate was discarded, and the filtrate was left for slow evaporation. After 4−5 days yellow needle crystals of the cocrystallized pair of complexes **1·2** were obtained (0.26 g, ∼45% yield). Anal. Calcd for $C_{106}H_{96}N_{34}O_{10}Cl_2Mn_4$: C, 55.43; H, 4.21; N, 20.73, Mn, 9.57. Found: C, 55.34; H, 4.16; N, 20.56; Mn, 9.62. IR (cm^{-1}): 2053 (s, sim. $\nu(N_3^-)$),[18,20,29] 1639 and 1590 (s, L1 ν(C═N)).

(ii) $[Mn_2(L2)_2(N_3)_2](ClO_4)_2$ (3). To a methanolic solution (10 mL) of $Mn(ClO_4)_2\cdot 6H_2O$ (0.09 g, 0.25 mmol) was added L2 (0.101 g, 0.25 mmol) in methanol (6 mL) over a period of 15 min. To the resulting yellow solution, an aqueous solution (6 mL) of sodium azide (0.016 g, 0.25 mmol) was added slowly. The solution was then filtered, an insoluble precipitate was discarded, and the filtrate was left for slow evaporation. After 3−4 days, orange needle-shaped crystals of **3** were obtained (0.040 g, ∼27% yield). Anal. Calcd for $C_{54}H_{48}N_{14}O_8Cl_2Mn_2$: C, 53.97; H, 4.03; N, 16.32, Mn, 9.14. Found: C, 53.88; H, 4.11; N, 16.21; Mn, 9.06. IR (cm^{-1}): 2049 (s, sim. $\nu(N_3^-)$),[18,20,29] 1633 and 1588 (s, L2 ν(C═N)).

(iii) $[Mn_2(L3)_2(N_3)_2](ClO_4)_2$ (4). Compound **3** was synthesized by slow addition of a methanolic solution (6 mL) of L3 (0.105 g, 0.25 mmol) to a methanolic solution (10 mL) of $Mn(ClO_4)_2\cdot 6H_2O$ (0.09 g, 0.25 mmol) with constant stirring for 45 min. To the resulting yellow solution, an aqueous methanolic solution of sodium azide (0.016 g, 0.25 mmol, 6 mL of H_2O, and 6 mL of MeOH) was added slowly with constant stirring for 15 min. The resulting solution after filtration was left to stand at room temperature, and after several days orange needle-shaped crystals of **3** were obtained (0.093 g, ∼61% yield). Anal. Calcd for $C_{56}H_{52}N_{14}O_8Cl_2Mn_2$: C, 54.68; H, 4.22; N, 15.94, Mn, 8.93. Found: C, 54.56; H, 4.17; N, 15.81; Mn, 8.86. IR (cm^{-1}): 2050 (s, sim. $\nu(N_3^-)$),[18,20,29] 1635 and 1587 (s, L3 ν(C═N)).

Caution! *Perchlorate salts and azido compounds are potentially explosive especially in the presence of organic compounds. They must be prepared and handled in small amounts with special care*.

Physical Measurements. Elemental analyses for carbon, hydrogen, and nitrogen were performed using a Perkin-Elmer 2400II elemental analyzer. Manganese contents were determined by titrimetric methods. Infrared spectra (4000−400 cm^{-1}) were recorded on KBr pellets (at 298 K) using a JASCO FT/IR-420 spectrometer. The magnetic studies were carried out on polycrystalline samples using a Quantum Design MPMS SQUID magnetometer operating in the 300−2 K temperature range and 0−5.5 T. Susceptibility measurements were performed within applied fields of 1000 Oe (**1·2** and **3**) or 5000 Oe (**4**). Pascal's constants were utilized to estimate diamagnetic corrections, the value in each case being subtracted from the experimental susceptibility data to give the molar magnetic susceptibility (χ_M).

X-ray Crystallography. Single crystals suitable for X-ray crystallographic analysis were selected in all cases following examination under a microscope. Single-crystal X-ray diffraction data for all compounds were collected on a Siemens SMART CCD diffractometer fitted with a graphite monochromator with Mo Kα radiation (λ = 0.710 73 Å) at 213(2) K with a detector distance of 4 cm and a swing angle of −35°. A hemisphere of reciprocal space covered by a combination of three sets of exposures; each set had a different ϕ angle (0, 88, 180°), and each exposure of 30 s covered 0.3° in ω. Data collection, indexing, and initial cell refinement were handled using SMART software.[30] Frame integration and final cell refinement were carried out using SAINT software.[31] The SADABS software package[32] was used to perform the absorption corrections. The atomic scattering factors are from the *International Tables for Crystallography*. The structure was solved by direct methods, completed by subsequent difference Fourier syntheses, and refined by full-matrix least-squares procedures on F^2 using SHELXTL.[33] The non-hydrogen atoms were refined anisotropically. The hydrogen atoms were refined with geometrical constraints with ideal bond lengths and angles and were treated as riding atoms. All computation were carried out on a PC using the SHELXTL-PC program package. The crystal data and data collection details are collected in Table 1.

Results and Discussion

Syntheses. Ligands L1−L3 were synthesized by refluxing ethylenediamine, 1,3-diaminopropane, or 1,4-diaminobutane, respectively, with 2 equiv of 2-benzoylpyridine in dehydrated alcohol, according to the known condensation reaction between a primary amine and a ketone. The yields were almost quantitative in all cases. The ligand L1 was allowed to react with equimolar amounts of manganese(II) perchlorate hexahydrate and sodium azide in aqueous methanol medium. This reaction afforded the yellow compound (**1·2**) formulated

(28) Deoghoria, S.; Sain, S.; Soler, M.; Wong, W. T.; Christou, G.; Bera, S. K.; Chandra, S. K. *Polyhedron* **2003**, *22*, 257.
(29) Nakamoto, K. *Infrared Spectra of Inorganic and Coordination Compounds*; Wiley: New York, 1997.
(30) *SMART*; Siemens Analytical X-Ray System: Madison, WI, 1996.
(31) *SAINT*; Siemens Analytical X-Ray System: Madison, WI, 1996.
(32) *SADABS*; University of Gottingen: Gottingen, Germany, 1996,.
(33) *SHELXTL*, version 5.1; Brucker Analytical X-Ray Systems: Madison, WI, 1997.

Table 1. Crystallographic Data for Complexes **1·2**, **3**, and **4**

	1·2	**3**	**4**
formula	$C_{106}H_{94}N_{34}O_{10}Cl_2Mn_4$	$C_{54}H_{48}N_{14}O_8Cl_2Mn_2$	$C_{56}H_{52}N_{14}O_8Cl_2Mn_2$
cryst size, mm	0.40 × 0.28 × 0.20	0.90 × 0.44 × 0.34	0.42 × 0.22 × 0.18
fw	2294.81	1201.16	1229.90
space group	$P\bar{1}$	*C*2/*c*	*C*2/*c*
a, Å	13.2206(2)	21.616(3)	21.616(3)
b, Å	13.3555(2)	17.6242(17)	17.6712(11)
c, Å	15.5049(1)	14.2932(18)	14.3505(9)
α, deg	72.902 (1)	90	90
β, deg	81.860 (1)	90.636(10)	91.933(1)
γ, deg	86.835(1)	90	90
V, Å^3	2590.04 (6)	5444.9(12)	5647.2(6)
Z	1	4	4
ρ_{calc}, g/cm^3	1.471	1.466	1.447
μ(Mo Kα), mm^{-1}	0.606	0.630	0.610
$\theta_{min}/\theta_{max}$, deg	1.7/25.0	1.70/28.00	2.31/25.00
indpnt reflcns	9030 (R_{int} = 0.0886)	6618 (R_{int} = 0.0874)	4959 (R_{int} = 0.0548)
obsd reflcns [$I > 2.0\sigma(I)$]	6062	4375	3481
R[a]	0.0686	0.0638	0.0830
R_w,[b] *S*	0.1840, 0.963	0.1589, 0.944	0.1594, 1.103

[a] $R = \Sigma(||F_o| - |F_c||)/\Sigma|F_o|$. [b] $wR = \{\Sigma w(|F_o|^2 - |F_c|^2)^2/\Sigma w(|F_o|^2)^2\}^{1/2}$.

as the pair of complexes $[Mn_2(L1)_2(N_3)_4][Mn_2(L1)_2(N_3)_2(CH_3OH)_2](ClO_4)_2$ on the basis of elemental analyses, infrared (IR) spectroscopy, and X-ray crystallographic data. The formation of this pair of cocrystallized complexes is striking. Since the Mn/N_3^- ratio in **1** is different from that in **2**, attempts of favoring the formation of either one or the other were made by repeating the reaction with different stoichiometries, the identity of the final product being invariably identified as composite **1·2**. As a possible reason for the favored cocrystallization of **1** and **2** as pairs of complexes is the presence in the solid state of a well-defined hydrogen bond between the terminal N_3^- group of **1** and the MeOH ligand of **2** (see below). The reaction of L2 and L3 respectively with manganese(II) perchlorate hexahydrate and sodium azide using the 1:1:1.5 ratio afforded the mutually related complexes $[Mn_2(L2)_2(N_3)_2](ClO_4)_2$ (**3**) and $[Mn_2(L3)_2(N_3)_2](ClO_4)_2$ (**4**), as orange crystalline products suitable for X-ray crystallographic analysis. As above, changing the ratio of the reagents did not lead to the formation of different products. The reason for the differences in structure (see below) and composition between **1·2** on one hand and **3** and **4**, on the other, probably lies on the structural requirements of the polydentate ligands. L1 is more rigid than L2 and L3 and leads to heptacoordination, a less common coordination geometry for Mn^{II}. The seventh coordination site is filled with terminal ligands (N_3^- or MeOH) allowing for the formation of a hydrogen-bonding network between **1** and **2** in the crystal lattice. On the contrary, the larger flexibility of L2 and L3 permits accommodation of the much more common six-coordinate environment around Mn^{II}, preventing the coordination of additional terminal ligands. Thus, the result in each case is the formation of one species in the solid state. The above observations underscore the significant differences in the coordination sphere around Mn, in composition of the products, and in the supramolecular organization in the solid state of these that can be caused by a seemingly irrelevant alteration of the ligand system.

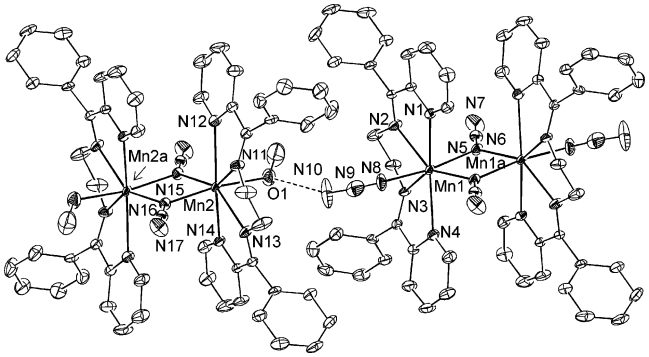

Figure 1. ORTEP representation at the 50% probability level of compound **1·2**, where the asymmetric unit and the Mn atoms are labeled, emphasizing the hydrogen-bonding interation between complexes **1** and **2**. For clarity, the hydrogen atoms are not shown.

Description of Structures

$[Mn_2(L1)_2(N_3)_4][Mn_2(L1)_2(N_3)_2(CH_3OH)_2](ClO_4)_2$ (1·2). An ORTEP representation of the crystallographic molecular structure of compound **1·2** is shown in Figure 1, while selected interatomic distances and angles are listed in Table 2. The unit cell of **1·2** consists of a pair of two different centrosymmetric dinuclear complexes of Mn^{II}, where the metal ions are chelated by the tetradentate ligand L1 and bridged by two N_3^- groups in an end-on fashion. A seventh coordination site is occupied by a terminal ligand N_3^- (complex **1**) or MeOH (complex **2**) completing an uncommon heptacoordinate environment around the Mn^{II} ions (MnN_7 for **1** and MnN_6O for **2**; see Figure 2). Thus, complexes **1** and **2** are mutually linked in the solid state by a hydrogen bond interaction established between the hydroxide group from the MeOH ligand in **1** and the terminal N_3^- ligand of **2** (O−H···N distance of 2.722(5) Å), forming infinite one-dimensional chains of weakly linked and alternated molecules of these two complexes. Molecule **1** is neutral, while the positive charges from the complex cation in **2** are balanced by two perchlorate ions. The coordination geometry around Mn(1) and Mn(2) is a close to a pentagonal bipyramid (see below) with axial positions occupied by the pairs of donor atoms [N(5);N(8)] for Mn(1) and [O(1);N(15)]

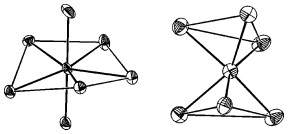

Figure 2. Drawing of Mn and its first coordination sphere for complexes **1** (left) and **3** (right) as emphasizing the quasi pentagonal bipyramid and trigonal prism, respectively, to which the coordination geometry on Mn in this report approximate. Mn is the central atom. Lines between non-manganese atoms are not chemical bonds.

Table 2. Selected Interatomic Distances (Å) and Angles (deg) for Compound **1·2**

Mn(1)−N(1)	2.465(3)	Mn(1)−N(2)	2.361(4)
Mn(1)−N(3)	2.365(3)	Mn(1)−N(4)	2.479(3)
Mn(1)−N(5)	2.241(3)	Mn(1)−N(8)	2.208(4)
Mn(1a)−N(5)	2.257(3)	Mn(2)−O(1)	2.208(3)
Mn(2)−N(11)	2.494(4)	Mn(2)−N(12)	2.325(3)
Mn(2)−N(13)	2.337(4)	Mn(2)−N(14)	2.466(3)
Mn(2)−N(15)	2.214(3)	Mn(2a)−N(15)	2.258(3)
Mn(1)···Mn(1a)	3.5091(7)	Mn(2)···Mn(2a)	3.4780(7)
O(1)−Mn(2)−N(11)	83.16(12)	O(1)−Mn(2)−N(12)	88.59(13)
O(1)−Mn(2)−N(13)	82.38(14)	O(1)−Mn(2)−N(14)	82.49(12)
O(1)−Mn(2)−N(15)	171.96(15)	O(1)−Mn(2a)−N(15)	104.88(11)
N(11)−Mn(2)−N(12)	67.06(12)	N(11)−Mn(2)−N(13)	135.13(11)
N(11)−Mn(2)−N(14)	150.25(10)	N(11)−Mn(2)−N(15)	104.77(12)
N(11)−Mn(2a)−N(15)	79.50(12)	N(12)−Mn(2)−N(13)	70.32(13)
N(12)−Mn(2)−N(14)	138.20(12)	N(12)−Mn(2)−N(15)	93.25(13)
N(12)−Mn(2a)−N(15)	142.23(14)	N(13)−Mn(2)−N(14)	68.05(11)
N(13)−Mn(2)−N(15)	90.86(14)	N(13)−Mn(2a)−N(15)	145.35(14)
N(14)−Mn(2)−N(15)	90.96(12)	N(14)−Mn(2a)−N(15)	79.22(12)
N(15)−Mn(2a)−N(15)	78.30(11)	Mn(2)−N(15)−Mn(2a)	101.70(12)
N(1)−Mn(1)−N(2)	67.60(11)	N(1)−Mn(1)−N(3)	137.45(10)
N(1)−Mn(1)−N(4)	154.07(10)	N(1)−Mn(1)−N(5)	87.50(12)
N(1)−Mn(1)−N(8)	85.92(12)	N(1)−Mn(1a)−N(5)	79.15(12)
N(2)−Mn(1)−N(3)	69.86(11)	N(2)−Mn(1)−N(4)	134.00(11)
N(2)−Mn(1)−N(5)	88.87(13)	N(2)−Mn(1)−N(8)	85.09(14)
N(2)−Mn(1a)−N(5)	144.57(14)	N(3)−Mn(1)−N(4)	66.32(10)
N(3)−Mn(1)−N(5)	90.75(11)	N(3)−Mn(1)−N(8)	91.51(11)
N(3)−Mn(1a)−N(5)	141.58(12)	N(4)−Mn(1)−N(5)	104.80(12)
N(4)−Mn(1)−N(8)	82.76(12)	N(4)−Mn(1a)−N(5)	81.37(12)
N(5)−Mn(1)−N(8)	172.39(15)	N(5)−Mn(1a)−N(5)	77.47(11)
N(8)−Mn(1a)−N(5)	104.98(11)	Mn(1)−N(5)−Mn(1a)	102.53(12)

for Mn(2). The bond distances to Mn are rather irregular, ranging from 2.208(4) to 2.479(3) Å and 2.208(3) to 2.494(4) Å for **1** and **2**, respectively. The shortest distances (2.208(3)−2.258(3) Å) correspond to bonds with bridging N_3^- groups or with the terminal ligands (see Table 2). The longest distances (to the polydentate ligand L1) fall within the range previously reported for other heptadentate Mn^{II} systems also including multidonor ligands.[34,35] The separations between manganese centers within the dinuclear units are 3.5091(7) (**1**) and 3.4780(7) Å (**2**), whereas the shortest intermolecular distance corresponds to the Mn(1)···Mn(2) vector and measures 8.1541(7) Å. The Mn−N−Mn bridging angles are 102.53(12) and 101.70(12)°, in complexes **1** and **2**, respectively.

$[Mn_2(L2)_2(N_3)_2](ClO_4)_2$ (3). The ORTEP representation of the cation of **3** is shown in Figure 3, whereas selected interatomic distances and angles are listed in Table 3. Complex **3** is a centrosymmetric bis(azido)-bridged dimer of Mn^{II} ions chelated by the tetradentate ligand L2, very similar to complexes **1** and **2**. The chief difference with the above systems is that, in **3**, the metals are six-coordinate and, therefore, do not possess terminal ligands. Consequently, no hydrogen bonds between molecules are observed like in the previous case. Charge neutrality within the system is ensured by the presence of two ClO_4^- ions/molecule. The MnN_6 coordination sphere observed in this complex is closer to the trigonal prism than to the octahedron (Figure 2; see below). The Mn−N(azido) distances are 2.204(3) and 2.276(3) Å, whereas the distances to N-donors from L2 range 2.229(2)−2.254(2) Å. This set of parameters are in line with previous observations on other MnN_6 chromophores.[36−38] The intermetallic distances are 3.5371(7) Å within the complex and 9.628 Å as the shortest Mn···Mn vector between molecules. The Mn−N−Mn angle within **3** measures 104.29(11)°.

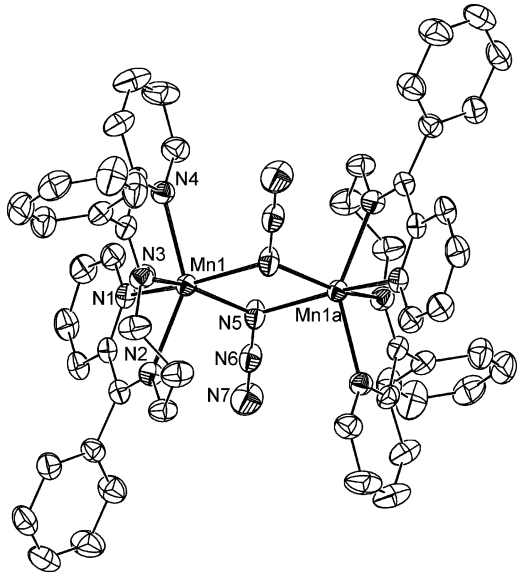

Figure 3. ORTEP representation at the 50% probability level of the complex cation of **3**, where the asymmetric unit and the Mn atoms are labeled. For clarity, the hydrogen atoms are not shown.

$[Mn_2(L3)_2(N_3)_2](ClO_4)_2$ (4). The molecular structure of the complex cation of **4** is represented in Figure 4, and the relevant metric parameters are collected in Table 3. Complex **4** is the analogue of **3** with ligand L3. Ligands L2 and L3 differ only in that the latter has one more CH_2 group in the chain linking the imine functions. This induces only slight geometrical differences, while the overall structure of the cluster is conserved. Thus, the coordination geometry around Mn^{II} is also between octahedral and trigonal prismatic (see below), although closer to the octahedron than in **3**. The Mn−N distance ranges are 2.222(4)−2.275(5) Å (N_3^-) and 2.239(4)−2.263(4) Å (L3), whereas the shortest Mn···Mn distances are 3.5338(10) (intramolecular) and 10.076 Å (intermolecular). Complex **4** features a bridging Mn−N−Mn angle of 103.58(19)°.

Continuous Shape Measures (CShM). Crystallographic studies on complexes **1**−**4** have revealed quite uncommon or far from ideal coordination geometries around Mn^{II} (Figure

(34) Deroche, A.; MorgensternBadarau, I.; Cesario, M.; Guilhem, J.; Keita, B.; Nadjo, L.; HoueeLevin, C. *J. Am. Chem. Soc.* **1996**, *118*, 4567.
(35) Sra, A. K.; Sutter, J. P.; Guionneau, P.; Chasseau, D.; Yakhmi, J. V.; Kahn, O. *Inorg. Chim. Acta* **2000**, *300*, 778.
(36) Lumme, P.; Mutikainen, I.; Lindell, E. *Inorg. Chim. Acta* **1983**, *71*, 217.
(37) Vos, G.; Haasnoot, J. G.; Verschoor, G. C.; Reedijk, J.; Schaminee, P. E. L. *Inorg. Chim. Acta* **1985**, *105*, 31.
(38) Ross, S.; Weyhermuller, T.; Bill, E.; Wieghardt, K.; Chaudhuri, P. *Inorg. Chem.* **2001**, *40*, 6656.

Table 3. Selected Interatomic Distances (Å) and Angles (deg) for Compounds **3** and **4**, in the **3/4** Format

Mn(1)−N(1)	2.254(2)/2.242(4)	Mn(1)−N(2)	2.232(2)/2.263(4)
Mn(1)−N(3)	2.229(2)/2.239(4)	Mn(1)−N(4)	2.240(2)/2.263(4)
Mn(1)−N(5)	2.204(3)/2.222(4)	Mn(1a)−N(5)	2.276(3)/2.275(5)
Mn(1)···Mn(1a)	3.5371(7)/3.5338(10)	N(1)−Mn(1)−N(2)	73.14(9)/73.06(14)
N(1)−Mn(1)−N(3)	113.15(9)/105.19(15)	N(1)−Mn(1)−N(4)	92.13(9)/91.11(14)
N(1)−Mn(1)−N(5)	87.05(9)/89.12(16)	N(1)−Mn(1)−N(5a)	157.65(9)/160.14(16)
N(2)−Mn(1)−N(3)	81.28(9)/85.13(14)	N(2)−Mn(1)−N(4)	142.90(9)/148.91(15)
N(2)−Mn(1)−N(5)	90.99(9)/88.61(17)	N(2)−Mn(1)−N(5a)	120.51(9)/119.32(16)
N(3)−Mn(1)−N(4)	73.48(9)/73.18(15)	N(3)−Mn(1)−N(5)	154.75(9)/161.89(16)
N(3)−Mn(1)−N(5a)	87.53(9)/91.89(15)	N(4)−Mn(1)−N(5)	122.77(9)/118.40(17)
N(4)−Mn(1)−N(5a)	85.57(9)/84.12(16)	N(5)−Mn(1)−N(5a)	75.71(9)/76.42(17)
Mn(1)−N(5)−Mn(1a)	104.29(11)/103.58(19)		

Table 4. Continuous Shape Measures (CShM) of the Coordination Geometry of Complexes **1**−**4** with Respect to Various Polyhedra[a]

	PBPY	C_{3v}-CO	C_{2v}-CTP	O	TP
1	1.64	5.18	3.91		
2	1.65	5.24	4.25		
3				7.61	3.21
4				5.65	4.76

[a] PBPY = pentagonal bipyramid; CO = capped octahedron; CTP = capped trigonal prism; O = octahedron; TP = trigonal prism.

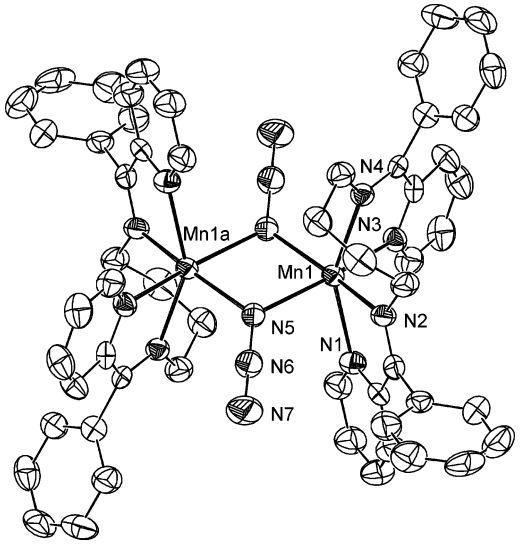

Figure 4. ORTEP representation at the 50% probability level of the complex cation of **4**, where the asymmetric unit and the Mn atoms are labeled. For clarity, the hydrogen atoms are not shown.

2). To describe in a rigorous quantitative manner the exact deviation of the coordination sphere of the different Mn^{II} ions from ideal polyhedra, we have performed CShM on all them.[39] The CShM of a given molecular polyhedron with respect to an ideal shape is a root-mean-squares minimized distance function from the first to the latter, calculated in a 0−100 scale. This value tends thus to zero as the actual polyhedron approaches the ideal one. In Table 4 are summarized all such measurements made in this study on the Mn ions from all compounds in this report. The CShM of seven-coordinate Mn(1) and Mn(2) in compound **1·2** revealed that their coodination geometry is closer to a pentagonal bipyramid (PBPY) than to any other seven-vertexes polyhedron. The distances to the C_{3v}-capped octahedron (CO) and to the C_{2v}-capped trigonal prism (CTP) have also been calculated and are much larger than to the PBPY. The measures for the six-coordinate Mn^{II} ions of **3** and **4** have shown that the coordination shape around these metals is, in both cases, between the perfect octahedron (O) and the trigonal prism (TP), although closer to the latter. Both distances are very similar, however, in complex **4**. Among the infinite pathways that can be followed in the process of transforming one polyhedron into another, a minimum distortion path can always be defined.[39] For example, the minimum distortion path for the interconversion between the octahedron and the trigonal prism is the Bailar twist, which consists on rotating by 60° two opposite faces of the octahedron around their C_3 axis. The distance of a distorted shape from the minimum distortion path linking two ideal polyhedra can be assessed by representing the CShM coordinates of the unperfect structure as a point on a symmetry map[40] of the two proposed perfect polyhedra where the minimum distortion path between them is also represented. Such representation for Mn of compounds **3** and **4** on the "octahedron versus trigonal prism" symmetry map shows that the coordination geometry of these ions lies very close to the distortion path of the Bailar twist (Figure S1). On the other hand, association of the distortion of Mn(1) and Mn(2) in **1·2** to any minimal distortion path between seven-vertex polyhedra proved not possible.

Magnetochemistry. Among end-on μ-N_3^--bridged dinuclear Mn^{II} complexes, the family of compounds **1·2**, **3**, and **4** is only preceded by one example (see above).[27] Thus, this group of complexes can provide the first few data points of an incipient magneto−structural correlation with the aim of establishing links between structural parameters and magnetic properties within such category of compounds, in ways similar to what has been performed previously with families of Cu,[41] Ni,[42] or Fe[43] complexes, following the pioneering work of Hatfield and Hodgson.[44]

Magnetic Susceptibility Studies. Variable-temperature, bulk magnetization data were collected for complexes **1·2**, **3**, and **4** under a constant magnetic field of 1 kG (**1·2** and **3**) or 5 kG (**4**). The results are shown in Figures 5 and 6 in form of $\chi_M T$ vs T curves. In such plots, χ_M is the molar

(39) Casanova, D.; Cirera, J.; Llunell, M.; Alemany, P.; Avnir, D.; Alvarez, S. *J. Am. Chem. Soc.* **2004**, *126*, 1755.
(40) Pinsky, M.; Avnir, D. *Inorg. Chem.* **1998**, *37*, 5575.
(41) Thompson, L. K.; Mandal, S. K.; Tandon, S. S.; Bridson, J. N.; Park, M. K. *Inorg. Chem.* **1996**, *35*, 3117.
(42) Clemente-Juan, J. M.; Chansou, B.; Donnadieu, B.; Tuchagues, J. P. *Inorg. Chem.* **2000**, *39*, 5515.
(43) Gorun, S. M.; Lippard, S. J. *Inorg. Chem.* **1991**, *30*, 1625.
(44) Crawford, V. H.; Richardson, H. W.; Wasson, J. R.; Hodgson, D. J.; Hatfield, W. E. *Inorg. Chem.* **1976**, *15*, 2107.

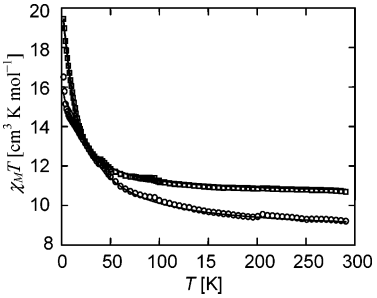

Figure 5. Plots of $\chi_M T$ vs T per mol of compounds **1·2** (squares) and **3** (circles). Solid lines are the best fits to the experimental data (see text for model and parameters).

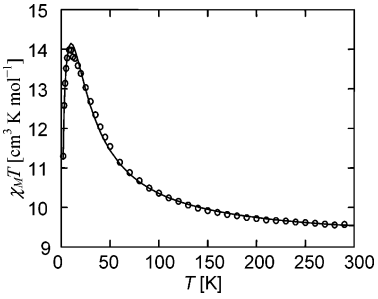

Figure 6. Plot of $\chi_M T$ vs T per mol for **4**. The solid line is the best fit to the experimental data modeling the low-temperature effects with intermolecular interactions.

paramagnetic susceptibility of the molecular complexes after being corrected for the diamagnetic contributions by use of Pascal's constants. Since data from cocrystallized compounds **1** and **2** cannot be separated, only the average for both is considered and discussed. The three sets of data show very similar behavior, only differing in the low-temperature effects. Thus, in all cases the value of $\chi_M T$ near 300 K is close to that expected for two uncoupled Mn^{II} ions/molecule (8.75 cm^3 K mol^{-1} for $g = 2$) and increases as the temperature diminishes to reach values near 14 cm^3 K mol^{-1} in the vicinity of 10 K. This behavior strongly indicates the presence of ferromagnetic coupling between the spin moments ($S_i = 5/2$) of the Mn^{II} ions within each dinuclear molecule to yield a total spin ground state of $S_T = 5$. It is clear, however, from the behavior at the lowest temperatures that effects operating in this range act differently for each compound. None of the compounds in this report display an apparent 3D network of weak intermolecular forces that would lead to bulk magnetic ordering below certain temperature; thus, the origin of possible intermolecular magnetic interactions (see below) must be of dipolar nature. Such type of interactions depends of the relative orientation of the magnetic centers, which is very different in each of the compounds studied (see Figure S2).

The pair of complexes **1·2** display an average value of $\chi_M T$ at 290 K of 10.7 cm^3 K mol^{-1} which stays nearly constant with decreasing temperature until approximately 100 K, from where it increases with growing (negative) slope up to 19.4 cm^3 K mol^{-1} at 2 K. This highest point is found well beyond the expected value (15 cm^3 K mol^{-1} for $g = 2$) for an $S_T = 5$ spin ground state, the largest possible molecular spin for this system. Thus, the experimental plot suggests the presence of ferromagnetic coupling between the $S_i = 5/2$ spins within the dinuclear complexes, accompanied by low-temperature intermolecular ferromagnetic ordering of the resulting $S_T = 5$ molecular spins. A model was used to fit the data, which included both types of magnetic interaction in addition to the Zeeman splitting, as reflected on the Hamiltonian $H = -2JS_1S_2 + g\mu_B S_{Tz}H - zJ'\langle S_{Tz}\rangle \boldsymbol{S}_{Tz}$. In this Hamiltonian, where all molecular spins in the compound are considered as identical, $S_i = 5/2$, $S_T = S_1 + S_2$, $\langle S_{Tz}\rangle$ is the expectation value of the spin component S_{Tz}, and zJ' is the coupling of the molecule with its z nearest neighbors, as equated using the molecular-field approximation.[45] From the above Hamiltonian, an expression for $\chi_M = f(T)$ derived from the Van Vleck equation[46] was obtained, by applying the Kambe vector coupling approach.[47] A least-squares numerical procedure was used to find the parameters J, zJ', and g that best allowed reproducing the experimental data (Figure 5). These were found to be 0.77(1) cm^{-1}, 0.010(3) cm^{-1}, and 2.198(3), respectively, which correspond the averaged values for complexes **1** and **2**, cocrystallized in this product. The value obtained for g is higher than expected for octahedral Mn^{II}. This discrepancy may be caused in part by the rare situation of heptacoordination observed in this compound or by the experimental error induced by the small uncertainty about the exact molecular mass of the measured compound, which is especially problematic when ligands from volatile solvents are present.

At 290 K, the product $\chi_M T$ for complex **3** has a value of 9.20 cm^3 K mol^{-1}, experiencing an increase in cooling, which is more pronounced than with the previous system. In this case, $\chi_M T$ tends to a plateau at approximately 9.20 cm^3 K mol^{-1} near 10 K before showing a new sharp increase up to 16.5 cm^3 K mol^{-1} at 2 K. This behavior can be interpreted in equivalent terms as for product **1·2**; thus, the same model as above was used to fit the data. In this case, however, a first fit of the data above 70 K was performed to obtain an accurate value of g (1.99(1)), which was then used as a fixed value to fit the entire curve and find the remaining parameters. The best fit (Figure 5) was obtained with the values 2.04(3) cm^{-1} and 0.008(1) cm^{-1} for J and zJ', respectively.

The experimental $\chi_M T$ vs T curve for complex **4** (Figure 6) displays an ordinate value of 9.56 cm^3 K mol^{-1} at 300 K that increases with diminishing temperatures to reach a maximum of 13.98 cm^3 K mol^{-1} at 10 K, followed by a sharp decrease to 11.30 cm^3 K mol^{-1} at 2 K. These observations are consistent with the presence of a $S_T = 5$ spin ground state for complex **4**, which, in contrast with the above complexes, experiences weak intermolecular antiferromagnetic ordering, leading to a decrease, rather than increase, of the $\chi_M T$ product at very low temperatures. Indeed, this was found numerically when the same model (which included intra- and intermolecular coupling) was used to fit the experimental data. Again, a suitable fit was obtained

(45) Kahn, O. VCH: New York, 1993; p 131.
(46) Van Vleck, J. H. *The Theory of Electric and Magnetic Susceptibilities*; Oxford Univesity Press: London, 1932.
(47) Kambe, K. *J. Phys. Soc. Jpn.* **1950**, *5*, 48.

when the g value arising from the calculation using the higher temperature range ($T > 12$ K, $g = 2.04(1)$) was included as a fixed parameter during the least-squares procedure performed with the whole data range. This led to best parameters of $J = 1.75(2)$ cm^{-1} and $zJ' = -0.054(1)$ cm^{-1}, yielding the fit represented in Figure 6 (solid line). The decrease of $\chi_M T$ at the lowest temperatures could also be interpreted as resulting from the presence of zero-field splitting (ZFS) of the molecular spin ground state. Thus, the data were fit to a model which contemplated this energy splitting of the ground state instead of the intermolecular interaction. For this, an expression of χ_M as a function of T was obtained on the basis of the Van Vleck equation resulting from the Heisenberg spin Hamiltonian of a dinuclear system ($H = -2JS_1S_2$) with the energies of the ground state ($S_T = 5$) modified by a ZFS term of the form $H_{ZFS} = D[S_{Tz}^2 - S_T(S_T + 1)/3]$.[48] The calculation using this model afforded the best-fit parameters $g = 2.04(1)$, $J = 1.68(3)$ cm^{-1}, and $D = 0.060(1)$ cm^{-1}. The fit (not shown) is slightly less good than the previous one, and therefore, the latter was preferred. In fact, it is likely that both effects are present in this system; however, being very similar in energy, it is not possible to distinguish between the two.

Magneto−Structural Correlation. The above results are not surprising since azido ligands are known to generally propagate ferromagnetic coupling interactions between nickel(II), manganese(II), or copper(II) centers when bound in a μ-1,1 end-on mode. This issue has been addressed from the theoretical point of view for binuclear complexes by use of hybrid density functional (DFT) methods under the assumption that the value of J is mainly dependent on the energy gap between magnetic orbitals (SOMO's).[49] Following this work, it was concluded that there must exist a correlation between the extent and nature of the exchange and the structural parameters that exert the largest influence on this energy gap, most in particular, the M−N−M angle. Such correlation has been established experimentally for μ-1,1-N_3^--bridged Cu^{II} dinuclear complexes[50] in a very similar way as shown extensively for their μ-OH^--bridged analogues.[44] However, with the experimental data available to date, the predicted correlation for azido-bridged Ni^{II} compounds has not been clearly corroborated.[51] In the case of Mn^{II} dinuclear complexes, this structure−property relationship has not been tested to date since only one such compound had been reported hitherto.[27] This work offers three additional data points which were used in a first attempt to investigate this correlation. In Figure 7 is a plot of J versus the Mn−N−Mn bridging angle, θ, as measured for **1·2**, **3**, **4**, and the previously reported complex $[Mn(terpy)(N_3)_2]_2$.[27] The data used to construct this plot are summarized in Table 5. This plot is interesting in that it reveals a possible correlation between both parameters that approximates to a straight line, with J becoming more positive as θ becomes wider. By contrast, the average Mn−N distances, d, in this group of complexes are very similar (differences within a range of 0.02 Å) and, consequently, no relation between d and J was found. Superimposed on the plot of Figure 7 (solid line) is the straight line that best reproduces the J vs θ trend, as obtained from a linear regression of the experimental data. These results are largely consistent with the theoretical predictions. They are explained with the fact that with larger angles increases the overlap within antibonding orbitals, whereas the nonbonding orbitals remain essentially unaffected, thereby increasing the energy gap between SOMO's. It must be mentioned that, on these theoretical studies, significant deviations from linearity are only predicted for angles that differ strongly from these expected for stable structures. On the other hand, the magnitude of the observed ferromagnetic coupling is significantly smaller than calculated. This disparity, however, has been consistently encountered for all the Ni^{II} systems studied, as well as for the case of Mn^{II}, and the reasons for it remain to be elucidated. The linear regression calculated from the experimental data predicts a change from ferromagnetic to antiferromagnetic behavior at an angle of 101°. This crossover is predicted by DFT calculations to take place for a θ value of approximately 98°. The above results are to be taken with caution since the number of points in the study remains small and the ranges of angles investigated and of J's observed are narrow. In addition, one of the experimental systems represents the average of two compounds. However, they possibly represent an important beginning in the understanding of the mechanism by which this ferromagnetic exchange is achieved and structural requirements leading to it. The preparation and study of additional systems of this category will be instrumental to confirm the trend observed here and, eventually, in helping to reduce the gap between the theoretical predictions and the experimental findings.

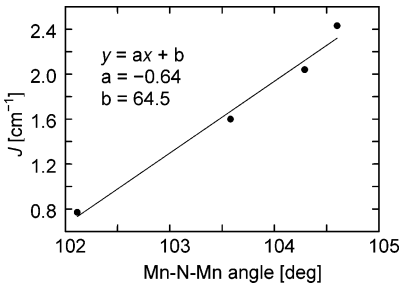

Figure 7. Plot of J vs θ (average Mn−N−Mn angle) for compounds **1·2**, **3**, **4**, and their reported congener.[27] The straight line is the best linear fit to the experimental values.

Table 5. Fit Parameters of the Complexes Discussed in the Text and Average Mn−N−Mn Angles

complex	J, cm^{-1}	zJ', cm^{-1}	g	θ, deg
1·2	0.77(1)	0.010(3)	2.198(3)	102.12[b]
3	2.04(3)	0.008(1)	1.99(1)	104.29(11)
4	1.75(2)	−0.054(1)	2.04(1)	103.58(19)
lit.[a]	2.43		2.0	104.60

[a] Previously reported. [b] Average between **1** and **2**.

(48) Kahn, O. VCH: New York, 1993; p 17.
(49) Ruiz, E.; Cano, J.; Alvarez, S.; Alemany, P. *J. Am. Chem. Soc.* **1998**, *120*, 11122.
(50) Tandon, S. S.; Thompson, L. K.; Manuel, M. E.; Bridson, J. N. *Inorg. Chem.* **1994**, *33*, 5555.
(51) Halcrow, M. A.; Sun, J. S.; Huffman, J. C.; Christou, G. *Inorg. Chem.* **1995**, *34*, 4167.

Concluding Remarks

Small geometric differences within newly synthesized imine−pyridine ligands lead to a change from hepta- to hexacoordination of the metal in a family of four dinuclear Mn^{II} complexes bridged by μ-η^1-N_3^- (end-on) ligands, with important consequences in composition and supramolecular organization of the molecular products. The ferromagnetic nature of the superexchange within the $[Mn_2(\mu\text{-}\eta^1\text{-}N_3)_2]$ moiety has been confirmed in all compounds, as had been observed on the only preexisting example. This feature could be exploited in future attempts of preparing higher nuclearity Mn^{II} clusters as potential new SMMs. A linear relationship has been observed between the measured Mn−N−Mn bridging angle of the complexes and their magnetic exchange coupling constant, which is consistent with predictions from theoretical DFT calculations. This experimental finding could be an important first step in the confirmation, with future examples, of a magneto−structural correlation within the category of (end-on) azido-bridged Mn^{II} complexes.

Acknowledgment. This work was supported by grants from the Council of Scientific and Industrial Research (Grant No. 01(1836)/03/EMR-II) and the Department of Science and Technology, New Delhi (Grant No. SR/S1/IC-22/2003), Government of India. T.K.K. thanks University Grants Commission, New Delhi, for a teacher fellowship. H.-K.F thanks the Malaysian Government and Universiti Sains Malaysia for research Grant R&D No. 305/PFIZIK/610961. G.A. thanks the Spanish Ministry of Science and Technology for a "Ramón y Cajal" research contract. The authors are thankful to Jordi Cirera (Universitat de Barcelona) for continuous shape measure calculations.

Supporting Information Available: X-ray crystallographic files in CIF format for complexes **1·2**, **3**, and **4**, symmetry maps of complexes **3** and **4** (Figure S1), and relative orientation of the magnetic centers for complexes **1**−**4** (Figure S2). This material is available free of charge via the Internet at http://pubs.acs.org.

IC048542V